Research in Astronomy and Astrophysics, 22:045009 (8pp), 2022 April https://doi.org/10.1088/1674-4527/ac538a

Optical and X-Ray Observations of MAXI J1820+070 During the Early Outburst Phase in 2018: Zooming in the Low Frequency QPOs*

Dong-Ming Mao[1,2], Wen-Fei Yu[1], Ju-Jia Zhang[3,4], Zhen Yan[1], Stefano Rapisarda[1], Xiao-Feng Wang[5,6], and Jin-Ming Bai[3,4]
[1] Shanghai Astronomical Observatory, Chinese Academy of Sciences, Shanghai 200030, China; wenfei@shao.ac.cn
[2] University of Chinese Academy of Sciences, Beijing 100049, China
[3] Yunnan Observatories, Chinese Academy of Sciences, Kunming 650011, China
[4] Key Laboratory for the Structure and Evolution of Celestial Objects, CAS, Kunming 650216, China
[5] Physics Department, Tsinghua University, Beijing 100084, China
[6] Beijing Planetarium, Beijing Academy of Sciences and Technology, Beijing 100044, China
Received 2021 November 29; revised 2022 January 17; accepted 2022 February 4; published 2022 March 17

Abstract

We report a further investigation of the optical low frequency quasi periodic oscillations (LF QPOs) detected in the black hole transient MAXI J1820+070 in the 2018 observations with the YFOSC mounted on Lijiang 2.4 m telescope (LJT). In addition, we make use of the Insight-HXMT/HE observations to measure the properties of the quasi-simultaneous X-ray LF QPOs of MAXI J1820+070 on the same day. We compared the centroid frequency, the full width at half maximum (FWHM) and the fractional rms of the LF QPOs in both wavelength ranges. We found that the centroid frequency of the optical QPO is at a frequency of 51.58 mHz, which is consistent with that of the X-ray LF QPO detected on the same day within 1 mHz. We also found that the FWHM of the optical LF QPO is significantly smaller than that of the X-ray LF QPO, indicating that the optical QPO has a higher coherence. The quasi-simultaneous optical and the X-ray LF QPO at a centroid frequency of about 52 mHz suggests that the actual mechanisms of these LF QPOs as the Lense–Thirring precession should work in the vicinity of a radius of about 80–117 gravitational radii ($R_g = GM/c^2$, M is the mass of the black hole) from the black hole if the QPO frequency is related to a proxy of the orbital frequency in the accretion flow as the Lense–Thirring precession model suggests. Furthermore, the apparent higher coherence of the optical QPO favors that it is a more original signal as compared with the X-ray QPO.

Key words: X-ray stars – Low mass binary stars – X-ray transient sources

1. Introduction

Black hole X-ray binaries (BH XRBs) are critical to our understanding of accretion physics. The majority of BH XRBs in our galaxy are transients, which usually stay in quiescence with occasional outbursts lasting weeks to months (Chen et al. 1997; Yan & Yu 2015). Generally speaking, BH XRB transients undergo several different spectral states during their outbursts, which are mostly classified into the hard and soft states, as well as intermediate state or very high state, based on their X-ray energy spectra and temporal properties (Remillard & McClintock 2006; Belloni 2010). BH XRBs in the hard state show an X-ray energy spectrum dominated by a power-law component with a photon index of 1.4–2 and a high-energy cutoff around 100 keV. The power-law component is thought to be the result of reverse Compton scattering of soft X-ray photons in a hot electron cloud very close to the black hole (Dove et al. 1998; Gilfanov 2010). As the outburst evolves, most BH XRBs enter the soft state, in which the X-ray energy spectrum is dominated by a multi-temperature blackbody component with a peak temperature of about 1 keV. This soft component is commonly considered to originate in an optically thick but geometrically thin accretion disk (Shakura & Sunyaev 1973; Zhang et al. 1997; Gierliński et al. 1999; Belloni 2010; Belloni & Motta 2016). During a typical evolution of an outburst, BH XRBs may go through intermediate states (hard and soft intermediate state), during which their energy spectra and timing properties are in between hard and soft states (Belloni 2010).

X-ray timing observations reveal that BH XRBs have distinct X-ray temporal properties in different spectral states (Homan et al. 2001; Remillard & McClintock 2006; Belloni 2010). Such temporal properties are usually quantified by computing the fractional root-mean-square (fractional rms) and looking at the Fourier power spectrum of the light curve (van der Klis 1989a). The X-ray light curve of BH XRBs in the hard state is highly variable, with fractional rms of 20%–40% (Belloni & Stella 2014) and power spectrum dominated by band-limited noise (BLN) and quasi-periodic oscillation (QPO) (van der Klis 1989b; Belloni et al. 2002). In the soft state, the X-ray variability is weak (fractional rms ∼1%–5%,

* Supported by the National Natural Science Foundation of China.

Belloni et al. 2005, 2011; Belloni 2010; Motta et al. 2011) and the power spectrum is dominated by power-law noise (Miyamoto et al. 1994; Cui et al. 1997; Remillard & McClintock 2006; Gilfanov 2010).

QPOs in BH XRBs appear as relatively narrower peak in the X-ray power spectrum on top of broad band noise (van der Klis 1989b; Belloni et al. 2002; van Straaten et al. 2002; Ingram & Motta 2019). The QPOs with centroid frequency below 30 Hz, generally referred as low-frequency quasi-periodic oscillations (LF QPOs, Belloni 2010), have been detected in most black hole transients (Ingram & Motta 2019). LF QPOs are usually classified into types A, B, or C according to their characteristics (peak frequency, coherence, and amplitude) in association with overall power spectral evolution (Wijnands & van der Klis 1999; Casella et al. 2005; Motta et al. 2015). The type-A QPO is generally considered to occur in the soft state, with a small fractional rms and a broad profile at the typical centroid frequency of about 6–8 Hz. The type-B QPO usually occurs in the soft intermediate state, with a relatively higher variability and a narrow profile at a typical centroid frequency range of 5–6 Hz (Casella et al. 2005; Belloni & Motta 2016). Finally, type-C QPOs are the most common QPO type in BH transients. They are usually observed on top of BLN noise in hard and hard-intermediate states, with centroid frequency increasing from a few mHz to ∼10 Hz (e.g., Homan et al. 2005, and references therein). Among all the QPO types, type-C QPOs have the narrowest profiles and the highest amplitudes (fractional rms ∼20%, Motta et al. 2012).

LF QPOs have been also detected in the optical and infrared energy band. For example, Motch et al. (1983) discovered that an optical LF QPO at a frequency about 1/2 of the X-ray QPO frequency in their simultaneous X-ray/optical observations of GX 339−4, and Gandhi et al. (2010) have also detected optical LF QPOs of this source. Hynes et al. (2003) found the frequencies of ultra-violet and optical LF QPOs are the same as that of X-ray ones in XTE J1118+480 and suggested that they have a common origin. Kalamkar et al. (2016) first detected an infrared LF QPO in GX 339−4 and suggested that it is connected to the precession of the jet.

Despite the extensive timing studies performed on BH XRBs, the origin of LF QPOs is still controversial. One of the most promising physical scenario proposed to explain the complex QPO phenomenology is the Lense–Thirring precession of the hot accretion flow in the vicinity of the black hole (Stella & Vietri 1998; Ingram et al. 2009; Ingram & Done 2011; Ingram & Motta 2019). An alternative model proposed by Tagger & Pellat (1999) suggests that the X-ray LF QPO is connected to the accretion-jet instability (Rodriguez et al. 2002; Varnière et al. 2002). A statistical study on X-ray LF QPOs amplitudes in GRS 1915+105 by Yan et al. (2013) suggests that low-frequency QPOs may originate in the corona rather than the jet. Ma et al. (2021) found the X-ray LF QPO can contribute up to above 200 keV in the black hole transient MAXI J1820+070, and they suggested that the QPO originates from an X-ray jet near the black hole. The model proposed by Veledina et al. (2013) argued that optical QPO may originate from the hot accretion flow by the Lense–Thirring precession, with optical photons produced in the outer region of the flow. Instead, Veledina & Poutanen (2015) suggested that X-rays generated in the precessing accretion flow near the black hole irradiate on the outer accretion disk and then produce the optical photons.

Optical fast photometric observations are an important tool to investigate the connections between phenomena occurring close to the black hole and the accretion disk. This could provide fundamental hints to unveil the geometry of accretion onto black holes and to validate general relativity predictions in the region closest to the black hole (Hynes et al. 2003; Ingram & Motta 2019). An optical QPO in the black hole transient MAXI J1820+070 was discovered by the Lijiang 2.4 m Telescope (LJT) and the Yunnan Faint Object Spectrograph and Camera (YFOSC) on MJD 58209 (2018 April 1) (Yu et al. 2018b)—the first time an optical QPO in a BH transient was discovered by Chinese optical facilities. The low frequency of the optical QPO allows us to investigate the frequency limit of optical QPOs in BH XRBs and to study the connection between the optical and the X-ray LF QPOs in a broad frequency range. In this paper, we present a comparison of the optical and the X-ray LF QPOs in MAXI J1820+070 detected on the same day by the LJT/YFOSC and the Insight-Hard X-ray Modulation Telescope (Insight-HXMT). In Section 2, we introduce the quasi-simultaneous optical and X-ray observations and the corresponding data reductions. In Section 3, we present the optical and the X-ray data analysis and results, including the power spectral analysis and the comparison of the QPO properties. The last section is discussion and conclusion.

2. Observations and Data Reduction

MAXI J1820+070 was discovered as the optical transient ASASSN-18ey by the All-Sky Automated Survey for Supernovae (ASAS-SN) on 2018 March 6 (Denisenko 2018; Tucker et al. 2018). A few days later it was observed in the X-ray band by the Monitor of All-sky X-ray Image (MAXI) on 2018 March 11 (Kawamuro et al. 2018). The position of MAXI J1820+070 is at R.A. = 18:20:21.94, decl. = +07:11:07.19 (Gandhi et al. 2019), and its distance is estimated as 2.96 ± 0.33 kpc (Atri et al. 2020). As a BH XRB (Baglio et al. 2018; Torres et al. 2019, 2020), MAXI J1820+070 was very bright in both X-ray (e.g., Mereminskiy et al. 2018) and optical bands (e.g., Russell et al. 2018; Sai et al. 2021). LF QPOs in MAXI J1820+070 have been detected in both optical (Fiori et al. 2018; Yu et al. 2018a, 2018b; Zampieri et al. 2018) and X-ray (Buisson et al. 2018, 2019; Mereminskiy et al. 2018; Mudambi et al. 2020; Stiele & Kong 2020) bands.

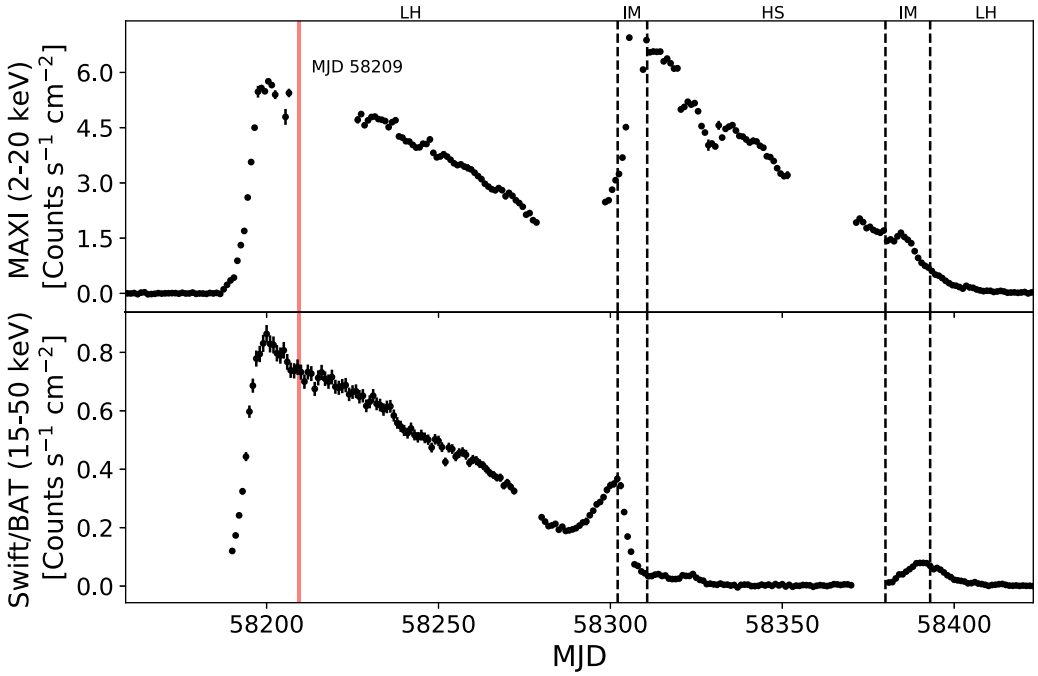

Figure 1. The monitoring light curves of MAXI J1820+070 by the MAXI and the Swift/BAT during the 2018 outburst. The black points represent the data with 1 day time bins. The red vertical line indicates that the optical and X-ray observation with the LJT/YFOSC and the Insight-HXMT on MJD 58209. The black vertical dashed lines show the X-ray spectral states of MAXI J1820+070 during its outburst (Shidatsu et al. 2019). "LH," "IM" and "HS" represent the hard state, the intermediate state and the soft state, respectively.

Figure 1 shows the daily averaged light curves during the 2018 outburst of MAXI J1820+070 monitored by the MAXI (2–20 keV) and the Swift/BAT (15–50 keV). The vertical dashed lines mark the X-ray spectral states—the low/hard state (LH), the intermediate state (IM) and the high/soft state (HS) (Shidatsu et al. 2019). The red vertical line indicates the day on which simultaneous observations were performed by the LJT/YFOSC and the Insight-HXMT. The source was in the hard state on that day.

2.1. Optical Observation with the LJT/YFOSC

High-cadence photometric observations of MAXI J1820+070 were obtained with the YFOSC installed on the LJT (Fan et al. 2015; Wang et al. 2019) on MJD 58208, 58209, and 58212. Of them, the observations spanned from 19:53:35 to 20:19:45 on MJD 58209 allowed the study of optical variability on a short timescale. For this observation, the exposure time of each exposure was set to 3 s, and the readout time of each frame is about 3.5 s. The total exposure time lasted for 1570 s, and a total of 240 images were obtained, with an average frame time of 6.58 ± 0.59 s. We used the standard LJT/YFOSC photometric program to obtain the flux of MAXI J1820+070 relative to the averaged flux of the total comparison stars near the target. We finally obtained the light curve with a time resolution of ~6.58 s, shown in Figure 2.

2.2. X-Ray Observation with the Insight-HXMT/HE

The Insight-Hard X-ray Modulation Telescope (Insight-HXMT) was launched on 2017 June 15 as the first X-ray astronomical satellite of China (Zhang et al. 2020). Insight-HXMT has a broad energy band and high time resolution with three main instruments, namely High Energy X-ray telescope (HE, ~20–250 keV, Liu et al. 2020), Medium Energy X-ray telescope (ME, ~5–30 keV, Cao et al. 2020), and Low Energy X-ray telescope (LE, ~1–15 keV, Chen et al. 2020). The time resolutions of the three instruments are 25 μs (HE), 280 μs (ME), and 1 ms (LE), respectively.

Two Insight-HXMT observations (ObsID: P0114661010 and P0114661 011) of MAXI J1820+070 starting at 20:41:00 on MJD 58208 and 20:33:19 on MJD 58209 (UTC) are the observations closest to the LJT/YFOSC optical observations. The total exposure times are 18,209 s and 68,997 s, respectively. We used Insight-HXMT Data Analysis Software (HXMTDAS, v2.0) for the data reduction and analysis of these two observations by applying the following suggested criteria: (1) elevation angle $< 10°$; (2) geomagnetic cutoff rigidity >8 GeV; (3) pointing offset angle $< 0.^{\circ}04$; (4) the time when Insight-HXMT passed the South Atlantic Anomaly (SAA) $> 300''$. The observation P0114661011 consists of five exposures, and we select the two exposures (P011466101101 and P011466101102) that are the closest to the LJT/YFOSC

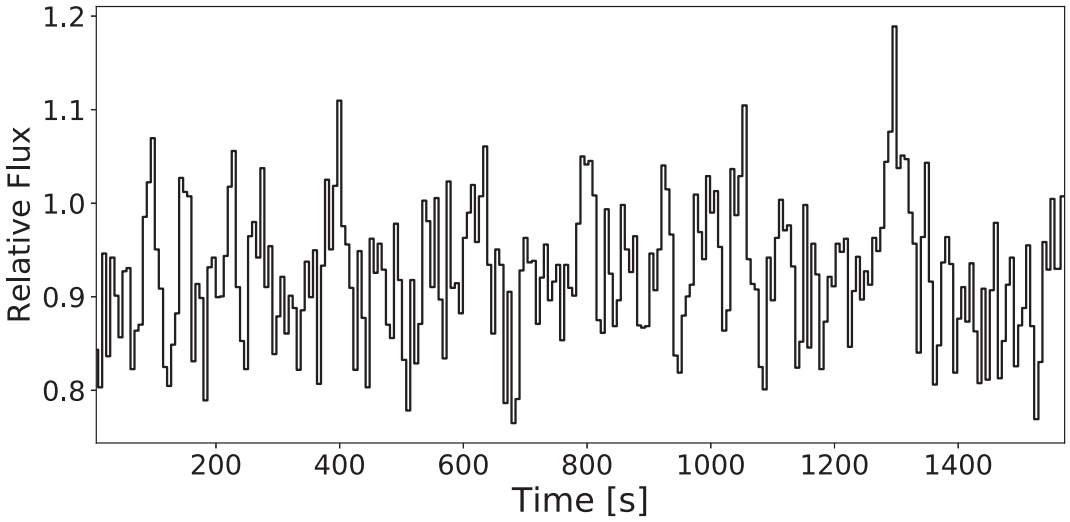

Figure 2. The optical light curve of MAXI J1820+070 obtained by the LJT/YFOSC on MJD 58209.

Table 1
The Measurement of the Parameters of the Optical and X-Ray LF QPOs in MAXI J1820+070

Telescope/ Instrument	ObsID	MJD	ν_0 (mHz)	FWHM (mHz)	Rms (%)	χ^2/dof
LJT/YFOSC	ToO	58209.83	$51.58^{+1.36}_{-1.09}$	$4.20^{+4.58}_{-3.00}$	$2.64^{+0.54}_{-0.53}$	17.3/26
Insight-HXMT/HE	P0114661010	58208.86	$55.96^{+1.04}_{-1.21}$	$4.38^{+3.38}_{-3.62}$	$6.40^{+1.04}_{-1.03}$	269.6/288
Insight-HXMT/HE	P0114661011	58209.86	$51.72^{+2.65}_{-3.73}$	$16.58^{+9.73}_{-6.00}$	$9.69^{+1.51}_{-1.18}$	336.4/288
Insight-HXMT/HE	P0114661011	58209.98	$55.63^{+1.02}_{-1.49}$	$10.23^{+5.02}_{-3.08}$	$8.63^{+1.18}_{-0.67}$	322.1/285

Note. All errors correspond to 1σ.

optical observation. The observation P0114661010 has an exposure window from 20:41 on MJD 58208 to 1:44 on the next day. P0114661011 had two exposure windows from 20:33 to 20:37 and from 23:37 to 4:08 on MJD 58209. The HE is capable of the highest time resolution for the X-ray detection in the high-energy band among the three detectors. Our data reduction of the X-ray LF QPO is similar to that in Ma et al. (2021). We used Insight-HXMT/HE results for the following power spectral analysis and comparison of the optical and X-ray LF QPOs, due to its larger averaged count rate.

In addition, the Swift/XRT observation (ObsID 00010627021) starting at 09:35:04 on MJD 58209 is also close to the optical observation. We included the result of the QPO detected in this observation (see ATEL#11510: Yu et al. 2018b) in the subsequent comparison analysis.

3. Data Analysis and Results

3.1. The Optical and X-Ray Power Spectral Analysis

We investigated optical and X-ray variability of MAXI J1820+070 and the connection between them by Fourier power spectral analysis. we divided the optical light curve with the duration of ∼1570 s (see Figure 2) into continuous 421 s segments, computed the power spectrum by fast Fourier transform for each time segment and averaged all of them. The power spectrum computed in this way has a frequency resolution ∼0.002 Hz and a Nyquist frequency of ∼0.076 Hz. As the low Nyquist frequency does not allow to measure the contribution of the white noise in a region where no variability is expected, we fixed the white level to a constant value by fitting. The X-ray power spectra were generated from the 20–250 keV X-ray light curves of the Insight-HXMT/HE divided into time segments of 262 s with the time bin size of ∼0.001 s. We used the average power above 800 Hz as an estimate of the white noise level in the X-ray power spectra. Both the optical and X-ray power spectra were rms normalized (see Belloni et al. 2002, for example).

We fit the optical and X-ray power spectra with a model composed of a zero-centered Lorentzian plus several additional Lorentzians to take into account the possible QPO components (Belloni et al. 2002; van Straaten et al. 2002). The reduced χ^2 of the best fit results is about 0.7–1.2. Table 1 shows the

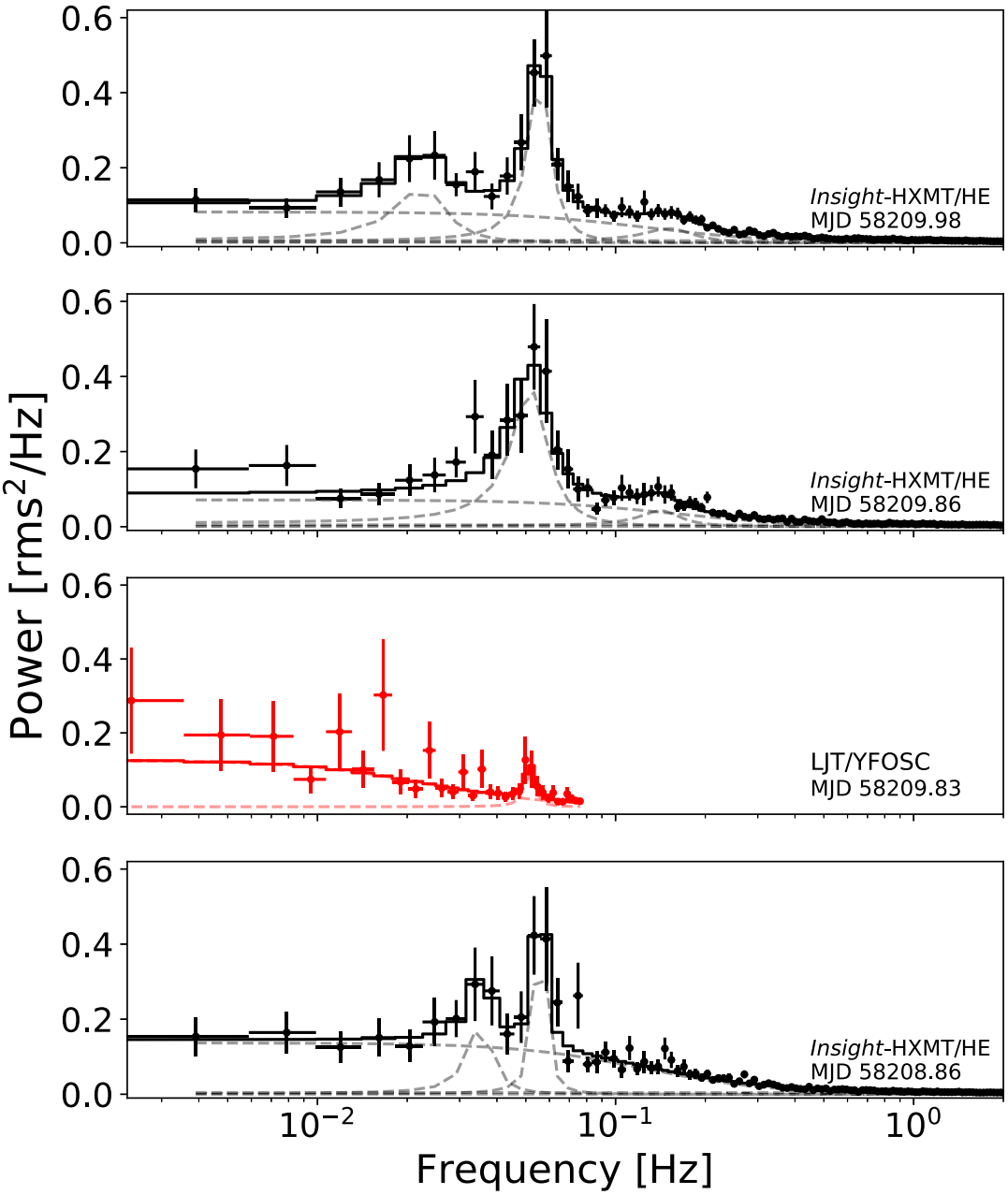

Figure 3. The optical and X-ray power spectra of MAXI J1820+070 within one day. The solid lines represent the power spectra (rms normalized) and fitting results of LJT/YFOSC (red) and Insight-HXMT/HE (black), respectively. The dashed lines represent the components in the power spectral fitting. The observation time is shown on the right side of each panel, and the earliest observed power spectrum is displayed at the bottom panel, and later ones are shown in upper panel in proper sequence. The time difference between the LJT/YFOSC observation and the nearest Insight-HXMT/HE observation is about 43 minutes, and the QPO centroid frequencies of these two bands are almost the same. In order to display each power spectrum more clearly and be convenient to compare them, we use the logarithmic coordinate for the *X*-axis and the linear coordinate for the *Y*-axis.

LJT/YFOSC and Insight-HXMT/HE observation time, the centroid frequency (ν_0), the full width half maximum (FWHM) and the fractional rms of the QPOs obtained in the power spectral fitting. Our results of the QPO measurements are shown in Table 1.

Figure 3 shows the optical and X-ray power spectra of MAXI J1820+070 obtained by LJT/YFOSC and Insight-HXMT/HE around MJD 58209. It can be seen that the X-ray power spectra of MAXI J1820+070 are similar to that of a typical BH XRB in the hard state. It consists of a BLN

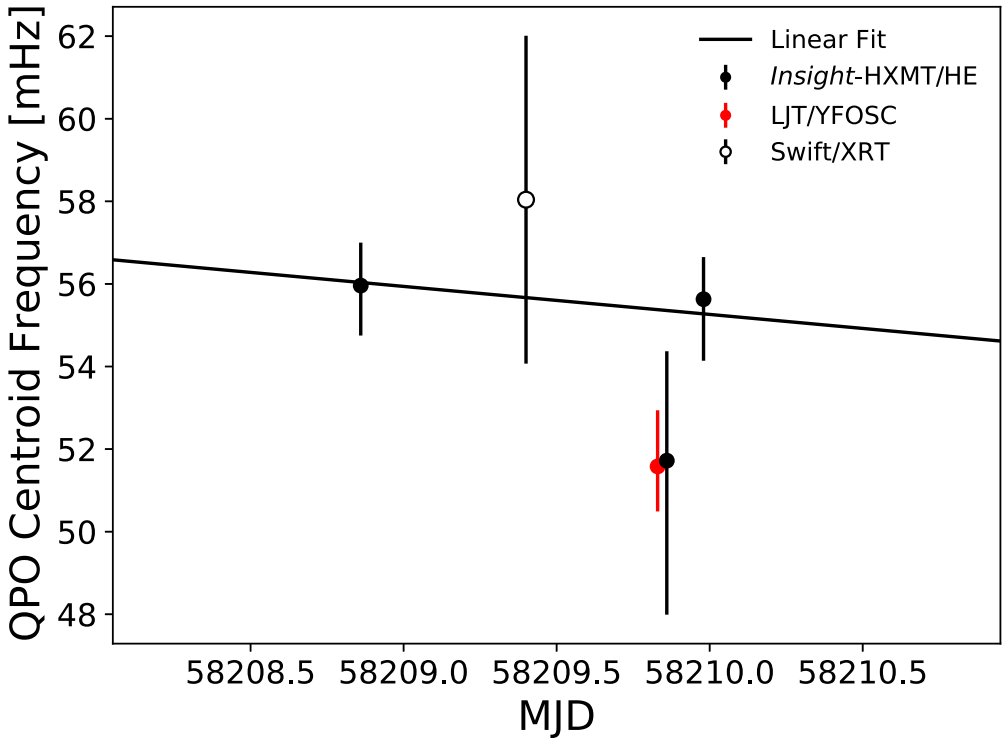

Figure 4. The evolution of the optical and X-ray LF QPOs centroid frequency in MAXI J1820+070 around one day. The black solid line represents the linear fitting of the X-ray QPO centroid frequency (ν_0) to the observation time (t) of the Insight-HXMT/HE and the Swift/XRT ($\nu_0 = -0.68^{+1.90}_{-1.74}(t - t_0) + 55.94^{+1.05}_{-1.06}$, $t_0 =$ MJD 58209).

component and a QPO signal. The optical power spectrum of MAXI J1820+070 has a quite similar feature to the X-ray power spectra, with the centroid frequencies of the optical and X-ray QPOs are almost the same. The similarity between optical and X-ray power spectra quasi-simultaneously observed in the black hole transient MAXI J1820+070 suggests that the optical and X-ray variability are likely connected. The similarity between the two powers may suggest a common origin, but a deep investigation of this possibility with more appropriate tools (such as cross-correlation) is beyond the scope of this work.

3.2. Comparison of the Optical and X-Ray Low-frequency QPO

To investigate the connection between the optical and the X-ray LF QPOs in MAXI J1820+070, we first compared the centroid frequency of the nearest optical/X-ray LF QPOs. We found that the difference between them is $0.14^{+2.98}_{-3.89}$ mHz (see Figure 3 and Table 1). It can be seen that the frequency down to 51.58 mHz of the optical QPO in MAXI J1820+070 is consistent with that of the X-ray QPO. Our LJT/YFOSC optical observation time does not match exactly the HXMT/HE X-ray observation time, so we considered three HXMT/HE X-ray observations and a Swift/XRT observation (see ATEL#11510: Yu et al. 2018b) as almost the same day with the optical. We fitted the QPO frequency trend in the X-ray band to check what the QPO frequency should be during our optical observation. Figure 4 shows the centroid frequencies of the optical/X-ray LF QPOs evolved with the observation time (MJD). The average of the frequency of X-ray QPOs detected by the quasi-simultaneous observations (including the three Insight-HXMT/HE observations and one Swift/XRT observation) on MJD 58209 is $55.34^{+1.25}_{-1.44}$ mHz, which differs from the optical QPO centroid frequency by $3.76^{+1.84}_{-1.81}$ mHz. We tentatively assume that the evolution of the QPO frequency in the X-ray band within one day can be well described by a linear form, thus the above X-ray QPO detection time versus centroid frequency can be fitted with $\nu_0 = a_0(t - t_0) + a_1$, where ν_0 is the QPO centroid frequency, t is the observation time of the QPO, $t_0 =$ MJD 58209, and a_0 and a_1 are the parameters to be fitted. The best fitting result gives $\nu_0 = -0.68^{+1.90}_{-1.74}(t - t_0) + 55.94^{+1.05}_{-1.06}$. The difference between the centroid frequency of the optical OPO and the X-ray one calculated from the above linear model is about 3.80 mHz. The centroid frequency at about 51.58 mHz of the optical LF QPO in MAXI J1820+070 is consistent with that of the X-ray QPOs within 4 mHz.

We further compared the FWHM and the fractional rms of the LF QPOs in MAXI J1820+070 in both bands. As shown in

Table 1 and Figure 3, the FWHM and the fractional rms of the optical LF QPO are both smaller than those of the quasi-simultaneous X-ray QPOs, and are about $1/2$ of the average FWHM and $1/3$ of the average fractional rms of the X-ray LF QPOs. The smaller FWHM of the optical QPO indicates that it has higher coherence than that of the X-ray QPOs, which suggests that the optical QPO may not be generated by the X-ray reprocessing and be likely from a more original signal.

4. Discussion and Conclusion

We re-analyzed the LJT/YFOSC optical observation of the black hole transient MAXI J1820+070 during the 2018 outburst (Yu et al. 2018b) in which the black hole optical LF QPO was detected and the Insight-HXMT/HE X-ray observations of MAXI J1820+070 performed on almost the same day in order to compare their centroid frequencies, FWHMs and fractional rms. We found that the centroid frequency of the optical LF QPO in MAXI J1820+070 was $51.58^{+1.36}_{-1.09}$ mHz, and the frequencies of the X-ray QPOs were $55.96^{+1.04}_{-1.21}$ mHz, $51.72^{+2.65}_{-3.73}$ mHz and $55.63^{+1.02}_{-1.49}$ mHz, respectively. The centroid frequency of the optical LF QPO differs from that of the X-ray QPO by $0.14^{+2.98}_{-3.89}$ mHz. By assuming a linear evolution occurring in the centroid frequency of the X-ray QPOs within one day, the centroid frequency of the optical LF QPO is consistent with that of the X-ray LF QPO. The independent measurements of consistent frequencies of the optical/X-ray LF QPOs in MAXI J1820+070 indicate that the optical and X-ray LF QPOs are linked.

The optical/infrared/ultra-violet LF QPOs with same centroid frequency as that of the X-ray LF QPO (or $1/2$ of the X-ray QPO frequency) and similar evolving trend (Hynes et al. 2003) have also been observed in several BH XRBs, such as GX 339−4 (Motch et al. 1983; Imamura et al. 1990; Gandhi et al. 2010; Kalamkar et al. 2016), XTE J1118+480 (Hynes et al. 2003) and SWIFT J1753.5−0127 (Durant et al. 2009). These phenomena suggest that the optical/infrared/ultra-violet LF QPOs might originate from the same physical mechanism responsible for the X-ray LF QPO. One of the most promising model for explaining the origin of the LF QPO is the Lense–Thirring precession of the hot accretion flow near the black hole (Stella & Vietri 1998; Ingram et al. 2009; Ingram & Done 2011; Ingram & Motta 2019). The hot accretion flow model proposed by Veledina et al. (2013) suggests that both the optical and X-ray LF QPOs originate from the precessing accretion flow, of which the outer region generates the optical photons. In an alternative X-ray reprocessing model, Veledina & Poutanen (2015) propose that the accretion flow produces the X-rays near the black hole. The optical emission comes from the irradiation of the X-ray in the outer region of the accretion disk. Thus the optical variability is modulated by the X-ray and presents the LF QPO with the same frequency as the X-ray. Our results show that, in the black hole transient MAXI J1820+070, the centroid frequency down to about 51.58 mHz of the optical LF QPO is consistent with that of the X-ray QPO detected on the same day. One way to investigate the relation between X-ray and optical QPO is by cross-correlating the light curves in these two energy bands. Unfortunately, our optical observations happened to be not exactly simultaneous with the X-ray data. By extrapolating the centroid frequency trend in the X-ray band, we compared the optical QPO centroid frequency with the best fit value at the detection time of the optical QPO, and found that these two values are consistent within a difference of about 4 mHz. This seems to suggest that the centroid frequencies of the optical and the X-ray LF QPOs are consistent within uncertainties, nevertheless, more accurate investigation is necessary to validate this preliminary conclusion.

In addition, we found that both the FWHM and the fractional rms of the optical LF QPO were smaller than those of the quasi-simultaneously observed X-ray QPOs, with the optical-X-ray ratio being $1/2$ for the averaged FWHM and $1/3$ for the averaged fractional rms, respectively.

Following the trend of increasing frequency of the LF QPO in MAXI J1820+070, Yu et al. (2018a) later used the LJT and the Fast Optical Camera (FOC) on 2018 April 22 (MJD 58230) to perform photometric observations of the black hole binary MAXI J1820+070 on the sub-second timescales and confirmed the consistency of the optical and the X-ray QPOs at ∼160 mHz. This indicates that the centroid frequency of the optical QPO in MAXI J1820+070 increased by a factor of about three in three weeks while remaining consistent with the centroid frequency of the X-ray LF QPO. These observations, together with our study, add important constrains on models aiming on explaining the complex LF QPO phenomenology in BH XRBs. The centroid frequency down to about 51.58 mHz of the optical QPO indicates that the Lense–Thirring precession model (see the equation in Ingram et al. 2009) should work within a radius of about 80–117 R_g from the black hole if the QPO frequency is a proxy of the orbital frequency in the accretion flow as suggested in the Lense–Thirring scenario, assuming that the compact object is a 8.48 solar mass black hole (Torres et al. 2020) with a spin of 0.3–0.998 and the surface density of the hot accretion flow is constant, and the threefold increasing of frequency means that the radius of the Lense–Thirring precession changes by about 1.9 times (up to $\sim 175R_g$).

The ratio of the QPO centroid frequency to the FWHM is generally called the quality factor ($Q = \nu_0/\mathrm{FWHM}$), which describes the coherence of the QPO signal, i.e., the timescale on which the QPO waveform remain coherent. As Barret et al. (2005) showed, the coherence timescale of a QPO signal is estimated as $\tau = Q/(\pi\nu_0) = 1/(\pi \cdot \mathrm{FWHM})$. Our results indicate that the optical LF QPO has consistent centroid frequency as that of the X-ray, but a smaller FWHM, indicating that the optical LF QPO has higher coherence suggesting that its coherence time is longer. This implies that the optical LF QPO

cannot be generated due to the reprocessing and modulation of the X-ray emission from the hot accretion flow near the black hole, further suggesting that the optical QPO is likely produced by a more original process.

Acknowledgments

This work was supported in part by the National Natural Science Foundation of China (NSFC, Grant Nos. U1838203 and 11333005) and the National Program on Key Research and Development Project (Grant No. 2016YFA0400804). We acknowledge the support of the staff of the Lijiang 2.4 m telescope funded by the Chinese Academy of Sciences (CAS) and the People's Government of Yunnan Province. This work also used the data from the Insight-HXMT mission, which is funded by China National Space Administration and the CAS. J.Z. is supported by the NSFC (Grant Nos. 12173082 and 11773067), by the Youth Innovation Promotion Association of the CAS (Grant No. 2018081), and by the Ten Thousand Talents Program of Yunnan for Top-notch Young Talents. Z.Y. was supported by the NSFC (Grant Nos. 11773055 and U1938114), Youth Innovation Promotion Association of CAS (ids. 2020265). X.W. is supported by NSFC grants (12033003 and 11633002) and the Scholar Program of Beijing Academy of Science and Technology (DZ:BS202002).

ORCID iDs

Wen-Fei Yu https://orcid.org/0000-0002-3844-9677
Ju-Jia Zhang https://orcid.org/0000-0002-8296-2590

References

Atri, P., Miller-Jones, J. C. A., Bahramian, A., et al. 2020, MNRAS, 493, L81
Baglio, M. C., Russell, D. M., & Lewis, F. 2018, ATel, 11418, 1
Barret, D., Kluźniak, W., Olive, J. F., Paltani, S., & Skinner, G. K. 2005, MNRAS, 357, 1288
Belloni, T., Homan, J., Casella, P., et al. 2005, A&A, 440, 207
Belloni, T., Psaltis, D., & van der Klis, M. 2002, ApJ, 572, 392
Belloni, T. M. 2010, in States and Transitions in Black Hole Binaries, ed. T. M. Belloni (Berlin: Springer), 53
Belloni, T. M., & Motta, S. E. 2016, in Transient Black Hole Binaries, ed. C. Bambi (Berlin: Springer), 61
Belloni, T. M., Motta, S. E., & Muñoz-Darias, T. 2011, BASI, 39, 409
Belloni, T. M., & Stella, L. 2014, SSRv, 183, 43
Buisson, D., Fabian, A., Alston, W., et al. 2018, ATel, 11578, 1
Buisson, D. J. K., Fabian, A. C., Barret, D., et al. 2019, MNRAS, 490, 1350
Cao, X., Jiang, W., Meng, B., et al. 2020, SCPMA, 63, 249504
Casella, P., Belloni, T., & Stella, L. 2005, ApJ, 629, 403
Chen, W., Shrader, C. R., & Livio, M. 1997, ApJ, 491, 312
Chen, Y., Cui, W., Li, W., et al. 2020, SCPMA, 63, 249505
Cui, W., Heindl, W. A., Rothschild, R. E., et al. 1997, ApJL, 474, L57
Denisenko, D. 2018, ATel, 11400, 1
Dove, J. B., Wilms, J., Nowak, M. A., Vaughan, B. A., & Begelman, M. C. 1998, MNRAS, 298, 729
Durant, M., Gandhi, P., Shahbaz, T., Peralta, H. H., & Dhillon, V. S. 2009, MNRAS, 392, 309
Fan, Y.-F., Bai, J.-M., Zhang, J.-J., et al. 2015, RAA, 15, 918
Fiori, M., Zampieri, L., Burtovoi, A., et al. 2018, ATel, 11824, 1
Gandhi, P., Dhillon, V. S., Durant, M., et al. 2010, MNRAS, 407, 2166
Gandhi, P., Rao, A., Johnson, M. A. C., Paice, J. A., & Maccarone, T. J. 2019, MNRAS, 485, 2642
Gierliński, M., Zdziarski, A. A., Poutanen, J., et al. 1999, MNRAS, 309, 496
Gilfanov, M. 2010, in X-Ray Emission from Black-hole Binaries, ed. T. Belloni (Berlin: Springer), 17
Homan, J., Miller, J. M., Wijnands, R., et al. 2005, ApJ, 623, 383
Homan, J., Wijnands, R., van der Klis, M., et al. 2001, ApJS, 132, 377
Hynes, R. I., Haswell, C. A., Cui, W., et al. 2003, MNRAS, 345, 292
Imamura, J. N., Kristian, J., Middleditch, J., & Steiman-Cameron, T. Y. 1990, ApJ, 365, 312
Ingram, A., & Done, C. 2011, MNRAS, 415, 2323
Ingram, A., Done, C., & Fragile, P. C. 2009, MNRAS, 397, L101
Ingram, A., & Motta, S. 2019, NewAR, 85, 101524
Kalamkar, M., Casella, P., Uttley, P., et al. 2016, MNRAS, 460, 3284
Kawamuro, T., Negoro, H., Yoneyama, T., et al. 2018, ATel, 11399, 1
Liu, C., Zhang, Y., Li, X., et al. 2020, SCPMA, 63, 249503
Ma, X., Tao, L., Zhang, S.-N., et al. 2021, NatAs, 5, 94
Mereminskiy, I. A., Grebenev, S. A., Molkov, S. V., et al. 2018, ATel, 11488, 1
Miyamoto, S., Kitamoto, S., Iga, S., Hayashida, K., & Terada, K. 1994, ApJ, 435, 398
Motch, C., Ricketts, M. J., Page, C. G., Ilovaisky, S. A., & Chevalier, C. 1983, A&A, 119, 171
Motta, S., Homan, J., Muñoz Darias, T., et al. 2012, MNRAS, 427, 595
Motta, S., Muñoz-Darias, T., Casella, P., Belloni, T., & Homan, J. 2011, MNRAS, 418, 2292
Motta, S. E., Casella, P., Henze, M., et al. 2015, MNRAS, 447, 2059
Mudambi, S. P., Maqbool, B., Misra, R., et al. 2020, ApJL, 889, L17
Remillard, R. A., & McClintock, J. E. 2006, ARA&A, 44, 49
Rodriguez, J., Varnière, P., Tagger, M., & Durouchoux, P. 2002, A&A, 387, 487
Russell, D. M., Baglio, M. C., Bright, J., et al. 2018, ATel, 11533, 1
Sai, H., Wang, X., Wu, J., et al. 2021, MNRAS, 504, 4226
Shakura, N. I., & Sunyaev, R. A. 1973, A&A, 500, 33
Shidatsu, M., Nakahira, S., Murata, K. L., et al. 2019, ApJ, 874, 183
Stella, L., & Vietri, M. 1998, ApJL, 492, L59
Stiele, H., & Kong, A. K. H. 2020, ApJ, 889, 142
Tagger, M., & Pellat, R. 1999, A&A, 349, 1003
Torres, M. A. P., Casares, J., Jiménez-Ibarra, F., et al. 2019, ApJL, 882, L21
Torres, M. A. P., Casares, J., Jiménez-Ibarra, F., et al. 2020, ApJL, 893, L37
Tucker, M. A., Shappee, B. J., Holoien, T. W. S., et al. 2018, ApJL, 867, L9
van der Klis, M. 1989a, in NATO Advanced Study Institute (ASI) Series C, Vol. 262, Timing Neutron Stars, ed. H. Ögelman & E. P. J. van den Heuvel (New York: Kluwer Academic), 27
van der Klis, M. 1989b, ARA&A, 27, 517
van Straaten, S., van der Klis, M., di Salvo, T., & Belloni, T. 2002, ApJ, 568, 912
Varnière, P., Rodriguez, J., & Tagger, M. 2002, A&A, 387, 497
Veledina, A., & Poutanen, J. 2015, MNRAS, 448, 939
Veledina, A., Poutanen, J., & Ingram, A. 2013, ApJ, 778, 165
Wang, C.-J., Bai, J.-M., Fan, Y.-F., et al. 2019, RAA, 19, 149
Wijnands, R., & van der Klis, M. 1999, ApJ, 514, 939
Yan, S.-P., Ding, G.-Q., Wang, N., Qu, J.-L., & Song, L.-M. 2013, MNRAS, 434, 59
Yan, Z., & Yu, W. 2015, ApJ, 805, 87
Yu, W., Lin, J., Mao, D., et al. 2018a, ATel, 11591, 1
Yu, W., Zhang, J., Yan, Z., Wang, X., & Bai, J. 2018b, ATel, 11510, 1
Zampieri, L., Fiori, M., Burtovoi, A., et al. 2018, ATel, 11723, 1
Zhang, S. N., Cui, W., Harmon, B. A., et al. 1997, ApJL, 477, L95
Zhang, S.-N., Li, T., Lu, F., et al. 2020, SCPMA, 63, 249502